DOI: 10.61782/fa.2023.0614

forum acusticum 2023

USING EIGENMODE FORCING TO INVESTIGATE FLOW INSTABILITY MECHANISMS CAUSING WHISTLING SOUND

Andreas Wurzinger[1*] **Bernhard Mayr-Mittermüller**[2] **Manfred Kaltenbacher**[1]
Stefan Schoder[1]
[1] Institute of Fundamentals and Theory in Electrical Engineering, Graz University of Technology, Graz, Austria
[2] Otto Bock Healthcare Products GmbH, Vienna, Austria

ABSTRACT

In flow acoustical problem sets, there is typically a large disparity of scales between hydrodynamical and acoustical phenomena both in amplitude and spatial extent. This results in major difficulties for low Mach number and high Reynolds number applications, resolving both acoustic and flow fields in a compressible flow simulation and applying correct boundary conditions. Consequently, during the design process of flow guiding structures, flow, and acoustic fields are only investigated separately, or a forward coupled simulation workflow (standard hybrid aeroacoustic approach) is used. This methodology, however, fails to accurately predict any flow instability mechanism caused by back-coupling of the acoustic field to the flow field, as is the case for whistling sound. This work presents a novel approach to excite flow instabilities, such as the whistling mechanism by applying acoustical mode forcing on an otherwise incompressible flow simulation. This allows for optimal domain size and boundary conditions of the incompressible flow domain. Furthermore, in contrast to strong direct coupling of the flow and acoustic domains, all interpolation tasks can be performed a priori. The relatively low computational cost makes this method especially well applicable to the task of designing complex flow-guiding structures such that whistling is mitigated in an early development stage.

Keywords: *Flow acoustics, stability analysis, whistling potentiality, eigenmode forcing*

**Corresponding author*: *andreas.wurzinger@tugraz.at.*

1. INTRODUCTION

Inside technical devices with flowing media such as hydraulics, pneumatics, or cooling circuits, the fluid flow serves purposes such as force transmission, damping, and heat transport, among others. Consequently, due to the low Mach numbers that come with low flow speed and high speed of sound of liquids, incompressible Computational Fluid Dynamics (CFD) is mostly used in the early design stage. Regarding flow acoustics, incompressible CFD is commonly used to obtain acoustic sources for successive acoustic propagation simulation (e.g.: [1], [2]). This type of hybrid aeroacoustic simulation workflow [3] based on pure forward coupling of the flow field to the acoustic field can give accurate predictions of turbulence generated sound [4] as well as sound production due to vortex shedding [5]. However, during the early development stage, however, a rough estimate of the radiated broadband sound caused by turbulent flow, as well as the existence of vortex shedding causing tonal sound production, might be sufficient to assess the quality of the design regarding flow acoustics. Therefore, estimations of the average acoustic source power $\langle P_{\text{source}} \rangle$ are used, e.g. in [6]

$$\langle P_{\text{source}} \rangle = -\rho_0 \left\langle \int_\Omega (\boldsymbol{\omega} \times \boldsymbol{u}) \cdot \boldsymbol{v}^{\text{a}} \, \mathrm{d}\Omega \right\rangle ,$$

where $\langle \bullet \rangle$ denotes the temporal average. Alternatively, in duct systems, a scattering matrix can be used to form an eigenvalue problem to analyze the growth rate of linearized modes of the compressible flow [7].

In most flow problems, vortex shedding is triggered by the instability of a detached mixing layer or jet flow. This kind of flow instability is caused by the feedback of either the generated vortical structures, i.e., hydro-dynamical feedback, or the acoustic mode caused by the vortex shedding, i.e., flow-acoustical feedback. As the sound-generating mechanism has to be resolved, incompressible CFD can model hydro-dynamical feedback only. Consequently, incompressible CFD cannot fully depict the whistling potentiality of complex flow geometries.

To give a reliable assessment of the whistling potentiality, either compressible flow simulation, i.e., Direct Noise Computation (DNC), or a hybrid workflow incorporating forward- and back-coupling from the flow to the acoustic model is required. Due to the disparity of length scales in flow acoustics [8], [9], DNC poses high requirements regarding temporal and spatial resolution of the domain resulting in high computational cost. Similarly, back-coupling from the acoustic to the flow domain adds significant complexity, as flow and acoustic fields need to be solved simultaneously. Flow and acoustic solvers often work with different methods on different grids and use different time step sizes for improved performance. Consequently, interpolation techniques, temporal sub-stepping techniques, or iterative coupling might be required.

This work presents a method to assess the whistling potentiality regarding flow-acoustical feedback that relies solely on incompressible CFD and uses eigenmode forcing to trigger the potential instability mechanism. The used method is presented in Section 2. In Section 3, the method is applied to simulate a simple geometry resembling a closed organ pipe. Section 4 discusses the obtained results and the limitations of the presented method, and Section 5 concludes the presented work.

2. METHODOLOGY

This section presents a fully coupled hybrid aeroacoustic formulation based on [10]. Consequently, the acoustic part of the formulation is transformed into modal space, and decoupling is achieved by using an estimation approach for the mode scaling.

2.1 Governing Equations

Starting from the fully compressible conservation equations of mass, momentum, and energy, [10] derived a set of equations separating the acoustic and incompressible flow fields introducing corresponding coupling terms. This is done by splitting the flow velocity $\boldsymbol{u}$ into incompressible, i.e. mean and vortical, and acoustic parts

$$\boldsymbol{u} = \underbrace{\bar{\boldsymbol{u}} + \boldsymbol{u}^{\mathrm{v}}}_{\boldsymbol{u}^{\mathrm{ic}}} + \boldsymbol{v}^{\mathrm{a}} \,. \tag{1}$$

Similarly, pressure p and density ρ can be split into mean and fluctuating parts due to incompressible (denoted by superscript $^{\mathrm{ic}}$ or $'$) and acoustic (denoted by superscript $^{\mathrm{a}}$) distortions

$$\begin{aligned} p &= p_0 + p^{\mathrm{ic}} + p^{\mathrm{a}} \,. \\ \rho &= \rho_0 + \rho' + \rho^{\mathrm{a}} \,. \end{aligned} \tag{2}$$

2.1.1 Incompressible flow

Assuming isentropic condition of the medium, the incompressible flow can be described by

$$\nabla \cdot \boldsymbol{u}^{\mathrm{ic}} = 0 \tag{3}$$

$$\rho_0 \frac{\partial \boldsymbol{u}^{\mathrm{ic}}}{\partial t} + \rho_0 \nabla \cdot \left(\boldsymbol{u}^{\mathrm{ic}} \otimes \boldsymbol{u}^{\mathrm{ic}} \right) = - \nabla p^{\mathrm{ic}} + \nabla \cdot \boldsymbol{\tau} - \boldsymbol{Q} \tag{4}$$

with the viscous stress tensor $\boldsymbol{\tau}$ and the coupling term

$$\boldsymbol{Q} = \boldsymbol{\omega}^{\mathrm{ic}} \times \boldsymbol{v}^{\mathrm{a}} \tag{5}$$

where $\boldsymbol{\omega}^{\mathrm{ic}}$ is the vorticity of the incompressible flow.

2.1.2 Acoustics

The acoustic back-coupling term in Eq. (5) requires knowledge of the acoustic particle velocity $\boldsymbol{v}^{\mathrm{a}}$, which can be solved using any acoustic conservation equations like APE-1 formulation [11], which is used in [10], or acoustic wave equation like the Perturbed Convective Wave Equation (PCWE) [12]

$$\frac{1}{c_0^2} \frac{\mathrm{D}^2 \psi^{\mathrm{a}}}{\mathrm{D}t^2} - \Delta \psi^{\mathrm{a}} = - \frac{1}{\rho_0 c_0^2} \frac{\mathrm{D} p^{\mathrm{ic}}}{\mathrm{D}t}, \quad \frac{\mathrm{D}}{\mathrm{D}t} = \frac{\partial}{\partial t} + \bar{\boldsymbol{u}} \cdot \nabla \,. \tag{6}$$

The PCWE is a reformulation of the APE-2 formulation [11] for low Mach number flows neglecting entropy and heat sources as well as vortical mode coupling and is solved for the acoustic potential ψ^{a}

$$\nabla \psi^{\mathrm{a}} = \boldsymbol{v}^{\mathrm{a}}, \quad \frac{\mathrm{D} \psi^{\mathrm{a}}}{\mathrm{D}t} = \frac{p^{\mathrm{a}}}{\rho_0} \,. \tag{7}$$

2.2 Modal decomposition

As the acoustic field is modeled linearly, it can be decomposed by a superposition of orthogonal basis functions $\boldsymbol{x}_i$. Consequently, an approximation of order N is given by

$$\psi^{\mathrm{a}} \approx \sum_{i=1}^{N} \psi_i^{\mathrm{a}} \boldsymbol{x}_i \,. \tag{8}$$

Using the harmonic ansatz

$$\psi^{\mathrm{a}} = \tilde{\psi}^{\mathrm{a}} e^{j\omega t}, \quad p^{\mathrm{ic}} = \tilde{p}^{\mathrm{ic}} e^{j\omega t} \,, \tag{9}$$

where j is the complex unit, ω is the angular frequency and $\tilde{}$ represents harmonic quantities, Eq. (6) can be transformed into the frequency domain

$$k^2 \tilde{\psi}^{\mathrm{a}} + \Delta \tilde{\psi}^{\mathrm{a}} = \frac{j\omega}{\rho_0 c_0^2} \tilde{p}^{\mathrm{ic}} \tag{10}$$

neglecting mean flow and with the wave number $k = \frac{\omega}{c_0}$. To obtain a set of orthogonal basis functions, the corresponding eigenvalue problem

$$(A - \boldsymbol{I}\lambda)\tilde{\boldsymbol{x}} = 0, \quad A = \Delta, \quad \lambda = -k^2 \tag{11}$$

can be solved for eigenvectors $\tilde{\boldsymbol{x}}$. The physical field can be approximately reconstructed by the time-harmonic field by

$$\psi^{\mathrm{a}} \approx \sum_{i=1}^{N} \gamma_i \left[\Re(\tilde{\psi}^{\mathrm{a}}) \cos(\omega_i t) + \Im(\tilde{\psi}^{\mathrm{a}}) \sin(\omega_i t) \right] \tilde{\boldsymbol{x}}_i \tag{12}$$

with according scaling factors γ_i. Using the definition of the acoustic potential given in Eq. (7), a decomposition of the acoustic particle velocity is given by

$$\boldsymbol{v}^{\mathrm{a}} = \nabla \psi^{\mathrm{a}} = \sum_{i=1}^{N} \psi_i^{\mathrm{a}} \nabla \boldsymbol{x}_i. \tag{13}$$

2.3 Mode scaling

The scaling factors γ_i in Eq. (12) are the remaining coupling variable from the incompressible flow to the acoustic field and can't be evaluated straightforwardly. For verification, the scaling factors can be chosen such that the absolute value of the acoustic pressure fluctuation $\tilde{p}_i^{\mathrm{a}}$ approximates the amplitude of the Fourier transform of the compressible pressure p^{c} at the corresponding eigenfrequency ω_i

$$|\tilde{p}_i^{\mathrm{a}}| \approx |\mathcal{F}\{p^{\mathrm{c}}\}|_{\omega_i} \,. \tag{14}$$

This approximation is only valid in a region far from any distorted flow, so pressure fluctuations based on the incompressible flow can be neglected. Naturally, this estimation requires knowledge of the compressible field and therefore is not practicable regarding the methodology presented. However, evaluating the accuracy of the presented estimation method will be useful.

2.3.1 *Acoustic source power*

An estimate for the averaged acoustic source power is derived by Howe [13]

$$\langle P_{\text{source}} \rangle = -\rho_0 \left\langle \int_{\Omega} (\boldsymbol{\omega} \times \boldsymbol{u}) \cdot \boldsymbol{v}^{\mathrm{a}} \, \mathrm{d}\Omega \right\rangle \,, \tag{15}$$

where $\langle \bullet \rangle$ represents the temporal average, Ω is the flow domain, $\boldsymbol{\omega} = \nabla \times \boldsymbol{u}$ is the vorticity of the flow field, and $\boldsymbol{u}$ and $\boldsymbol{v}^{\mathrm{a}}$ are the flow and acoustic particle velocities, respectively.

This estimate can be simplified as shown by [6] arriving at

$$\langle P_{\text{source}} \rangle = \left\langle \int_{\Gamma} (B' \boldsymbol{m}') \cdot \boldsymbol{n} \, \mathrm{d}\Gamma \right\rangle \,, \tag{16}$$

with the fluctuating total enthalpy B' and the fluctuating mass flow $\boldsymbol{m}'$

$$B' = \frac{p^{\mathrm{a}}}{\rho_0} + \bar{\boldsymbol{u}} \cdot (\boldsymbol{v}^{\mathrm{a}} + \boldsymbol{u}^{\mathrm{v}}) \,, \tag{17}$$

$$\boldsymbol{m}' = \rho_0 (\boldsymbol{v}^{\mathrm{a}} + \boldsymbol{u}^{\mathrm{v}}) + \rho' \bar{\boldsymbol{u}} \,, \tag{18}$$

and acoustic pressure fluctuation p^{a}, mean flow velocity $\bar{\boldsymbol{u}}$, and fluctuating velocity of the vortical flow field $\boldsymbol{u}^{\mathrm{v}}$. Thereby, Γ_{a} represents a closed contour containing the investigated flow domain. If Γ_{a} is chosen to be far from the detached flow, the vortical flow field can be assumed to vanish, i.e., $\boldsymbol{u}^{\mathrm{v}} \to 0$. Furthermore, the contribution of the mean flow to the sound generation is neglected. Therewith, Eq. (16) simplifies to

$$\langle P_{\text{source}} \rangle \approx \left\langle \int_{\Gamma_{\mathrm{a}}} p^{\mathrm{a}} \boldsymbol{v}^{\mathrm{a}} \cdot \boldsymbol{n} \, \mathrm{d}\Gamma \right\rangle = \langle P_{\mathrm{a}} \rangle \tag{19}$$

which is the definition of acoustic power.

2.3.2 *Scaling factor estimation*

For the investigation of a singular dominant acoustic mode, the mode forcing can be written according to Eq. (7) and (12) as

$$p^{\mathrm{a}} \approx \gamma_1 p_1^{\mathrm{a}}\,, \quad \boldsymbol{v}^{\mathrm{a}} \approx \gamma_1 \boldsymbol{v}_1^{\mathrm{a}} \tag{20}$$

with scaling factor γ_1. The mode forcing shall be done in a way that the resulting acoustic source power and radiated sound power are of the same order of magnitude, and therefore, $\langle P_{\mathrm{source}} \rangle \stackrel{!}{=} \langle P_{\mathrm{a}} \rangle$. With Eq. (15), (19), and (20), this can be rearranged to give an estimate for the scaling factor

$$\gamma_1 \approx \frac{-\rho_0 \left\langle \int_\Omega (\boldsymbol{\omega} \times \boldsymbol{u}) \cdot \boldsymbol{v}_1^{\mathrm{a}} \,\mathrm{d}\Omega \right\rangle}{\left\langle \int_{\Gamma_{\mathrm{a}}} p_1^{\mathrm{a}} \boldsymbol{v}_1^{\mathrm{a}} \cdot \boldsymbol{n} \,\mathrm{d}\Gamma \right\rangle}\,. \tag{21}$$

As the acoustic field is curl-free, and with the assumption $\left|\boldsymbol{u}^{\mathrm{ic}}\right| \gg |\boldsymbol{v}^{\mathrm{a}}|$, the first term in the source integral of Howe is approximated by the incompressible quantities. Furthermore, the sound power of mode 1 is known a priori based on preliminary acoustic simulation. It has to be noted that the mean part of the acoustic power of the selected mode represents the effective power that is radiated. Therefore, the effective part of the acoustic intensity is used in the denominator of Eq. (21), i.e. $\langle p_1^{\mathrm{a}} \boldsymbol{v}_1^{\mathrm{a}} \rangle = \frac{1}{2} \Re \left(p_1^{\mathrm{a}} \boldsymbol{v}_1^{\mathrm{a}*} \right) = \boldsymbol{I}_{\mathrm{eff}}^{\mathrm{a}}$ with * marking the complex conjugate. Therewith, the scaling factor can be calculated by

$$\gamma_1 \approx C \left\langle \int_\Omega \left(\boldsymbol{\omega}^{\mathrm{ic}} \times \boldsymbol{u}^{\mathrm{ic}} \right) \cdot \boldsymbol{v}_1^{\mathrm{a}} \,\mathrm{d}\Omega \right\rangle \tag{22}$$

$$C = \frac{-2\rho_0}{\left| \int_{\Gamma_{\mathrm{a}}} \Re \left(p_1^{\mathrm{a}} \boldsymbol{v}_1^{\mathrm{a}*} \right) \cdot \boldsymbol{n} \,\mathrm{d}\Gamma \right|}\,. \tag{23}$$

3. SIMULATION SETUP

In order to demonstrate the applicability of the methodology, the flow of a simplified flute is investigated. The simulation setup resembles the setup of [14] that was used as a demonstrative example in [10]. To reduce the computational effort and focus solely on the flow-acoustical feedback mechanism, the geometry was simplified and projected to a 2D problem, as depicted in Fig. 1.

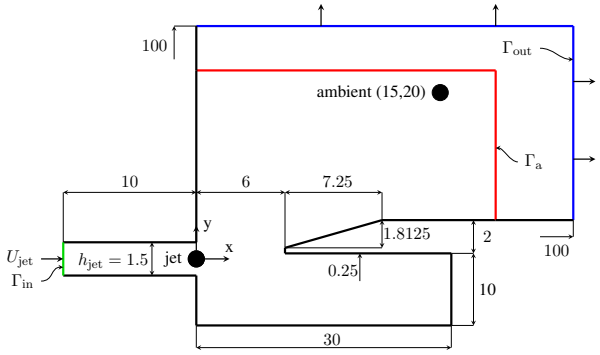

Figure 1. Not true to scale sketched geometry of a simplified flute with indicated evaluation points and flow boundary conditions. Dimensions in mm.

3.1 Preliminary acoustic simulation

To obtain the acoustic modes that ultimately cause vortex shedding by flow-acoustic feedback, the acoustic eigenmodes are calculated by solving the eigenvalue problem defined in Eq. (11). The domain was discretized by approximately 13000 first-order elements with a maximum size of $h_{\max} = 2\,\mathrm{mm}$. The boundaries to the ambient and at the jet inlet were chosen as sound hard to account for the reflections that occur at the boundaries of the reference simulation (see Sec. 3.3). However, this leads to a zero-valued constant following Eq. (22), as a closed system has no effective power. To circumvent this issue, the amplitude of the acoustic intensity $|\boldsymbol{I}^{\mathrm{a}}| = |p^{\mathrm{a}} \boldsymbol{v}^{\mathrm{a}}|$ is used instead of the effective acoustic intensity to calculate the acoustic power in Eq. (23), which will be discussed in Sec. 4. Used fluid properties are given in Tab. 2. The simulation was performed with the open source finite element solver *openCFS* [1]. Table 1 lists the first 4 eigenfrequencies of the problem set an the corresponding acoustic power evaluated according to Eq. (19) on the contour Γ_{a} as depicted in Fig. 1. As the acoustic particle velocity is zero on all walls, only the part of the contour that goes through the domain has to be evaluated. Modes 1 and 4 represent the first and second oscillation modes of the Helmholtz-resonator-like back-volume of the flute, while modes 2 and 3 are room modes due to the reflecting boundary conditions. It has to be denoted here that only mode 1 contributes significantly to the flow instability as their resulting particle velocity fields deflect the jet upstream to the trailing edge of the cavity. As the acoustic power indi-

[1] opencfs.org

cates, mode 4 is one order smaller in magnitude and consequently has no contribution to the whistling mechanism.

Table 1. Eigenfrequencies of the acoustic domain.

mode	frequency	acoustic power
1	1517 Hz	1.03×10^{-5} W
2	1765 Hz	2.36×10^{-6} W
3	2100 Hz	2.69×10^{-6} W
4	2700 Hz	1.39×10^{-6} W

3.2 Flow simulation

The flow simulation used the pressure-based incompressible flow solver available in *ANSYS Fluent*. The computational domain consists of approximately 27000 cells. At the inlet, a flow profile according to Poisseuille flow

$$U(y) = U_{\text{jet}} \left(\frac{y^2}{(h_{\text{jet}}/2)^2} - 1 \right) \tag{24}$$

is applied with peak jet velocity $U_{\text{jet}} = 30\,\text{m}\,\text{s}^{-1}$ and jet channel width $h_{\text{jet}} = 1.5\,\text{mm}$. This leads to a low Reynold's number flow at $\text{Re}_{h_{\text{jet}}} \approx 200$. Hence laminar flow can be assumed. At the ambient boundary, a pressure outlet is applied. All walls are modeled by no-slip boundaries, and the used fluid properties are given in Tab. 2. The mode forcing term is computed based on Eq. (5) using the first acoustic eigenmode at $f = 1517\,\text{Hz}$ according to Eq. (13) and scaled using Eq. (22). The temporal averaging was implemented using a moving mean operator with a window width $T_{\text{mean}} = 5 \times 10^{-3}\,\text{s}$. Figure 2 depicts the flow field at time $t = 0.05\,\text{s}$ when the flow reaches a state of steady oscillation.

Table 2. Fluid properties based on [10].

speed of sound	$c_0 = 343\,\text{m}\,\text{s}^{-1}$
density	$\rho_0 = 1.165\,\text{kg}\,\text{m}^{-3}$
kinematic viscosity	$\nu = 1.53 \times 10^{-4}\,\text{m}^2\,\text{s}^{-1}$
center jet velocity	$U_{\text{jet}} = 30\,\text{m}\,\text{s}^{-1}$

3.3 Verification simulation

A DNC using a fully compressible flow simulation is performed to verify the methodology. The air is therefore

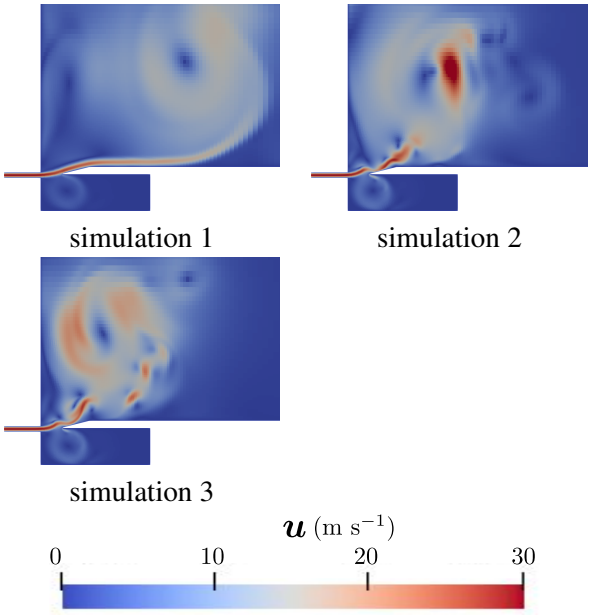

Figure 2. Velocity fields simulations 1 (incompressible), 2 (compressible), and 3 (mode forcing) at time $t = 0.05\,\text{s}$.

modeled as an ideal gas, with properties according to Tab. 3. By resolving both flow and acoustic features and therewith allowing full interaction a reference solution is obtained to compare the mode forcing method. The simulation is performed on the same grid and with the same boundary conditions as the incompressible flow simulation (see Sec. 3.2). For both, inlet and outlet boundaries, *non-reflecting boundary conditions* (NRBCs) were used to reduce reflections. However, significant reflections of acoustical waves were observed. Consequently, the acoustic simulation was adapted to match the far-field compressible pressure (see Sec. 3.1).

Table 3. Thermal fluid properties.

specific heat capacity	$c_p = 1006.43\,\text{J}\,\text{kg}^{-1}\,\text{K}^{-1}$
thermal conductivity	$\lambda = 0.0242\,\text{W}\,\text{m}^{-1}\,\text{K}^{-1}$
molecular weight	$M = 28.966\,\text{kg}\,\text{kmol}^{-1}$

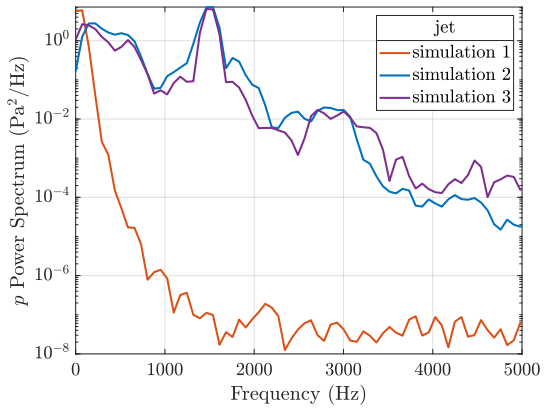

Figure 3. Power spectral density of the flow pressure at a monitoring point located inside the jet (see Fig. 1) for incompressible, compressible and mode forcing simulations.

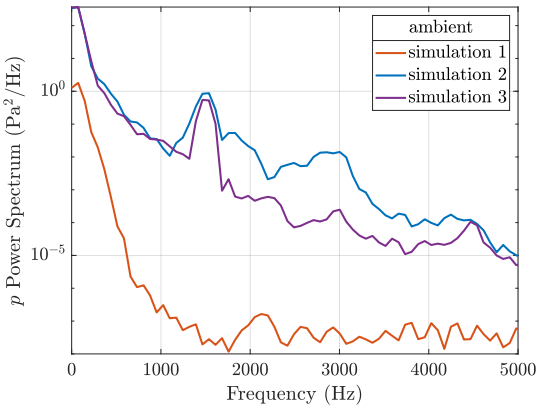

Figure 4. Power spectral density of the flow pressure at a monitoring point located above the cavity (see Fig. 1) for incompressible, compressible and mode forcing simulations.

4. DISCUSSION

The flow simulations were run for $T = 0.08\,\mathrm{s}$ and the flow pressure at the monitoring locations as indicated in Fig. 1 was evaluated in the interval $T_{\mathrm{eval}} = [0.05,\ 0.08]\,\mathrm{s}$.

Figures 3 and 4 depict the power spectral density (PSD) of the flow pressure at the monitoring points located in the jet and above the cavity as indicated in Fig. 1. The spectrum was obtained by Welch's method using a Hann window of size $T_{\mathrm{w}} = 0.01\,\mathrm{s}$ and 50% overlap. Simulation 1 is an incompressible simulation without mode forcing, simulation 2 a fully compressible reference simulation, and simulation 3 uses the presented methodology. For simulation 1, the incompressible pressure is evaluated, while for simulations 2 and 3, the compressible flow pressure is used. To obtain the compressible pressure for simulation 3, the oscillating pressure due to the acoustic eigenmode scaled by the estimated scaling factor is added to the incompressible flow pressure before evaluating the PSD. As expected, simulation 1 doesn't show any fluctuations, as the whistling mechanism is based on flow-acoustic feedback, which can't be modeled by incompressible fluid, and the jet attaches to the wall, and a laminar steady-state sets in due to the low Reynold's number. On the other hand, both simulations 2 and 3 show a distinct peak at around $1500\,\mathrm{Hz}$, which is the main whistling frequency. The pressure amplitude of the peak in simulation 3 is in good agreement with simulation 2, indicating appropriate scaling of the acoustic mode. However, one must remember that the forced mode used in this demonstrative example represents a standing wave instead of the physically correct radiating mode. Therefore, the scaling factor had to be estimated using the amplitude of the acoustic power instead of the effective one. This way, the mode scaling is not based on the radiated acoustic energy but on the reactive power amplitude.

Figure 5 shows the temporal evolution of the estimated scaling factor for simulations 1 and 3. Once the initial transient is faded away, the scaling factor estimate is negligible for simulation 1 while converging to a value of $\gamma_1 \approx 41.5$ in simulation 3. The fluctuation could be further reduced by extending the window length of the moving average filter. However, the simulation has proved to be insensitive to fluctuations in the scaling factor. This value is slightly lower than $\gamma_1 \approx 51.4$ one would obtain according to Eq. (14). This explains the slight underestimation of PSD in Fig. 4 at the whistling frequency and could be due to nonlinear effects and the simplifying assumptions made in Sec. 2. The pressure spectrum inside the jet region is also predicted accurately for higher frequencies. However, towards higher frequencies, simulation 3 underestimates the pressure fluctuations at the ambient monitor outside the flow region, as only one acoustic mode is included in the simulation, and therefore other compressible effects at other frequencies can't

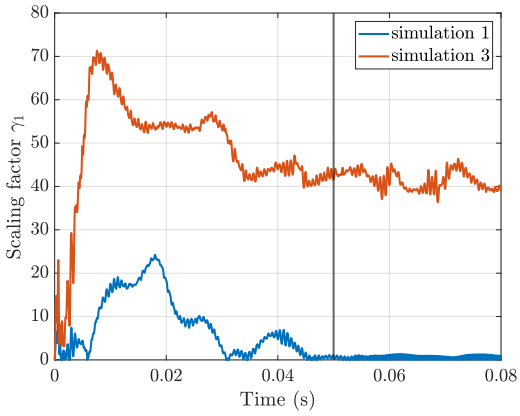

Figure 5. Temporal evolution of the scaling factor γ_1 for simulations 1 and 3.

be resolved.

5. CONCLUSION

The presented method combines incompressible flow simulations with acoustic eigenmode forcing using a hybrid formulation incorporating flow acoustic feedback. Consequently, the flow acoustic feedback mechanism, the main source of whistling noise, can be modeled. Due to the modal representation of the major acoustic mode, the acoustic domain can be solved a priori. Mode scaling of a single dominant mode can be achieved using an estimate for the acoustic source power, which can be evaluated straightforwardly during the incompressible flow simulation. The methodology allows triggering the vortex shedding of a jet flow impinging on an edge in a simple flute geometry, giving a good estimation of the flow pressure at the vortex shedding frequency. Significant deviations to the fully coupled simulation approach can be observed at higher frequencies as only one acoustic mode has been considered. In assessing the whistling potentiality of a certain flow configuration, these limitations are acceptable as the method still indicates correctly that a change of the flow guide is necessary to avoid the whistling sound. However, further investigation is needed to find a physical explanation of whether the used approximation of the radiated acoustic energy by the reactive power amplitude is a valid simplification. Furthermore, additional studies have to be done to investigate the robustness of the method in case of stable flows and other geometries need to be examined that give more significant insight into the general feasibility of the presented method.

6. ACKNOWLEDGMENTS

This project has received funding from the Austrian Research Promotion Agency (FFG) under the Bridge project No. [71694]. The computational results presented have been partially achieved using the software *openCFS*.

7. REFERENCES

[1] S. Schoder, C. Junger, and M. Kaltenbacher, "Computational aeroacoustics of the eaa benchmark case of an axial fan," *Acta Acustica*, vol. 4, no. 5, p. 22, 2020. DOI: 10.1051/aacus/2020021.

[2] S. Schoder, M. Weitz, P. Maurerlehner, *et al.*, "Hybrid aeroacoustic approach for the efficient numerical simulation of human phonation," *The Journal of the Acoustical Society of America*, vol. 147, no. 2, pp. 1179–1194, 2020.

[3] S. Schoder and M. Kaltenbacher, "Hybrid aeroacoustic computations: State of art and new achievements," *Journal of Theoretical and Computational Acoustics*, vol. 27, no. 04, p. 1 950 020, 2019. DOI: 10.1142/s2591728519500208.

[4] P. Maurerlehner, S. Schoder, J. Tieber, *et al.*, "Aeroacoustic formulations for confined flows based on incompressible flow data," *Acta Acustica*, vol. 6, p. 45, 2022. DOI: 10.1051/aacus/2022041.

[5] S. Schoder, A. Wurzinger, C. Junger, *et al.*, "Application limits of conservative source interpolation methods using a low mach number hybrid aeroacoustic workflow," *Journal of Theoretical and Computational Acoustics*, vol. 29, no. 01, p. 2 050 032, 2021. DOI: 10.1142/s2591728520500322.

[6] G. Nakiboğlu, S. Belfroid, J. Golliard, and A. Hirschberg, "On the whistling of corrugated pipes: Effect of pipe length and flow profile," *Journal of Fluid Mechanics*, vol. 672, pp. 78–108, 2011. DOI: 10.1017/s0022112010005884.

[7] A. Kierkegaard, S. Allam, G. Efraimsson, and M. Åbom, "Simulations of whistling and the whistling potentiality of an in-duct orifice with linear aeroacoustics," *Journal of sound and vibration*, vol. 331, no. 5, pp. 1084–1096, 2012. DOI: 10.1016/j.jsv.2011.10.028.

[8] T. Colonius, "Modeling artificial boundary conditions for compressible flow," *Annu. Rev. Fluid Mech.*, vol. 36, pp. 315–345, 2004. DOI: 10.1146/annurev.fluid.36.050802.121930.

[9] M. Piellard and B. Coutty, "Application of a hybrid computational aeroacoustics method to an automotive blower," in *Institution of Mechanical Engineers. Vehicle thermal management systems conference and exhibition (VTMS10). London: Heritage Motor Centre*, 2011. DOI: 10.1533/9780857095053.6.447.

[10] R. Ewert and J. Kreuzinger, "Hydrodynamic/acoustic splitting approach with flow-acoustic feedback for universal subsonic noise computation," *Journal of Computational Physics*, vol. 444, p. 110 548, 2021. DOI: 10.1016/j.jcp.2021.110548.

[11] R. Ewert and W. Schröder, "Acoustic perturbation equations based on flow decomposition via source filtering," *Journal of Computational Physics*, vol. 188, no. 2, pp. 365–398, 2003. DOI: 10.1016/s0021-9991(03)00168-2.

[12] M. Kaltenbacher, A. Hüppe, A. Reppenhagen, F. Zenger, and S. Becker, "Computational aeroacoustics for rotating systems with application to an axial fan," *AIAA journal*, vol. 55, no. 11, pp. 3831–3838, 2017. DOI: 10.2514/1.j055931.

[13] M. S. Howe, "The dissipation of sound at an edge," *Journal of Sound and Vibration*, vol. 70, no. 3, pp. 407–411, 1980. DOI: 10.1016/0022-460x(80)90308-9.

[14] H. Kühnelt, "Studying the vortex sound of recorder-and flute-like instruments by means of the lattice boltzmann method and helmholtz decomposition," Ph.D. dissertation, PhD thesis, University of Music and Performing Arts Vienna, 2016.